IEEE Access
Multidisciplinary | Rapid Review | Open Access Journal

Received 11 September 2022, accepted 9 October 2022, date of publication 12 October 2022, date of current version 19 October 2022.

Digital Object Identifier 10.1109/ACCESS.2022.3213982

RESEARCH ARTICLE

An Invasive Weed Optimization for Sensor Less Control of Grid Integrated Wind Driven Doubly Fed Induction Generator

ABHINAV SAXENA[1], (Member, IEEE), RAJAT KUMAR[2], (Member, IEEE), JAY SINGH[3], (Senior Member, IEEE), GYANENDRA KUMAR SINGH[4], V. SAMPATH KUMAR[5], AND J. P. PANDEY[6]

[1]Department of Electrical Engineering, JSS Academy of Technical Education, Noida, Uttar Pradesh 201301, India
[2]Department of Electrical and Electronics Engineering, Vardhaman College of Engineering, Hyderabad 501218, India
[3]Department of Electrical and Electronics Engineering, G. L. Bajaj Institute of Technology and Management, Greater Noida, Uttar Pradesh 201310, India
[4]School of Mechanical, Chemical & Materials Engineering, Adama Science and Technology University, Adama, Ethiopia, Adama 1888, Ethiopia
[5]Department of Electronics and Communication Engineering, JSS Academy of Technical Education, Noida, Uttar Pradesh 201301, India
[6]Department of Electrical Engineering, Madan Mohan Malaviya University of Technology, Gorakhpur, Uttar Pradesh 273016, India

Corresponding author: Gyanendra Kumar Singh (gksinghgu@yahoo.com)

ABSTRACT The article presents the design and development of invasive weed optimization (IWO) for the sensor less speed control of doubly fed induction generator (DFIG) under balanced and unbalanced conditions. A healthy condition represents the balanced condition while unbalancing condition is characterized by unhealthy conditions like three-phase fault, single line to ground fault, the line-to-line fault, and double line to ground fault. The DFIG is driven by wind and integrated with the grid. The advantages associated with IWO technique are a simple mathematical approach and less data computation. Normally, DFIG consists of two back-to-back converters namely grid side converter (GSC) and rotor side converter (RSC). The GSC is an uncontrolled converter while the RSC is a controlled converter. The existing methods have poor performance parameters like settling time, peak overshoot for balanced conditions, and poor power quality parameters like total harmonic distortion (THD) for unbalanced conditions. An IWO technique has been applied to overcome such limitations. The effectiveness of the sensor less speed control is also analyzed with other techniques like Adaptive Neuro-Fuzzy Interference System (AN-FIS) & artificial neural network (ANN). The design of ANN is based on the feed-forward method using back propagation delay and the design of ANFIS is based on adaptive control and state space control strategy. It is observed that performance parameters like peak overshoot and settling time for the sensor less speed of DFIG are found to be more profound with IWO in comparison to ANFIS, ANN, and other existing techniques for balanced conditions. Similarly in the unbalanced condition, faulty current approaches are quite closer to their healthy state with the IWO method in comparison to other methods. In addition to this, minimum distortion (%THD) for the grid current under unbalanced conditions is also attained with IWO in comparison to ANFIS, ANN, and other existing techniques. Such application of IWO makes the system highly efficient and robust.

INDEX TERMS AN-FIS, ANN, DFIG, GSC, IWO, RSC, sensor less.

I. INTRODUCTION

A doubly fed induction generator (DFIG) is a typical wound type induction machine in which the rotor is connected to the grid via RSC & GSC through DC-link while the stator is directly connected to the grid. The fault current assessment of DFIG in the unbalancing conditions is analyzed with different techniques in [1], [2], and [3]. The conventional approach for the sensor less control of DFIG for the balanced and unbalanced conditions under the application of solar and

The associate editor coordinating the review of this manuscript and approving it for publication was Zhuang Xu.

wind is also shown in [4], [5], [6], and [7]. Enhancing stability analysis & designing of the optimal controller, improvement of dc-link voltage & maximum power extraction, are also discussed tremendously [8], [9]. In [10], [11], the controlling of wind turbine for its maximum power extraction with the conventional methods are discussed. The tuning of controlling parameters of DFIG using various intelligent techniques [12], [13] & the advanced control strategy under FRT are well discussed in [14]. The optimal solution & robust control of internal parameters of DFIG under slide mode control & Lyapunov theory are quite well observed in [15], [16], and [17]. The methods like a deep-stacked auto encoder, convolution neural network, and deep belief network show too much variation in rotor position & speed of DFIG with the changes in the internal parameter. The traditional method of designing ANFIS for sensor less control of DFIG refer to [18] and [19] which give poor result in terms of higher settling time and more peak overshoot. Maximum power point tracking (MPPT) energy extraction from wind power-based DFIG under sensor less mode of operation is presented in [20] and [21]. The different control strategy which improves the DC link voltage of DFIG is shown in [22]. Some new control methods for a sensor less scheme of DFIG give unsatisfactory results which are shown in [23] and [24]. From all the above existing methods, basic issue observed is that sensor less speed and torque of DFIG has more peak overshoot and more settling time in balanced conditions & higher THD for unbalanced conditions. The concept of selecting sensor less speed over conventional speed to achieve more profound results is novel. Sensor less reduces the chances of getting error in the results due to the absence of effect vibration of shaft etc. The presence of shaft vibration effect and higher cost of sensor are the disadvantages of traditional method of speed measurement. The direct measurement of speed from current sensor only which is called as sensor less speed are advantages of proposed scheme. The most conclusive and significant information retrieved after analyzing the comprehensive and exhaustive literature review is that sensor less speed and torque has been able to rectify the issue of measurement of speed and torque with conventional sensor-based method but the techniques used in measurement and controlling of sensor less speed still giving the inappropriate results in terms of higher settling time, more peak overshoot, and highly distorted value. Such inadequate and higher distortion creates a problem to regain its original state after the elimination of fault. The similar kind of problems is also reflecting in [17] and [20]. In order to overcome the issue, the sensor less speed control of DFIG is assessed by using IWO for both balanced and unbalanced conditions which is the key point of this paper.

The design aspect of IWO is quite simpler in mathematical approach with less complexity. It also consumes less quantity of data which helps to enhance the speed of operation. The design of the IWO topology can be applied to any physical system for analyzing the performance parameters. The performance analysis of sensor less control of DFIG is also

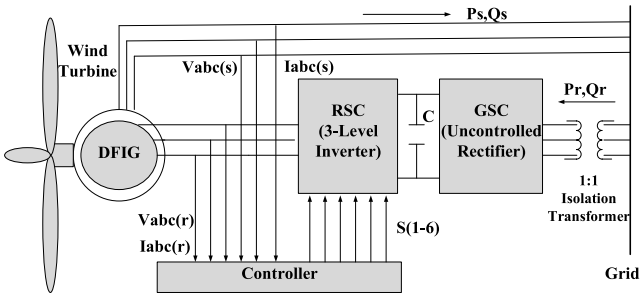

FIGURE 1. Power flow structure of DFIG.

analyzed with ANFIS, ANN, and other existing methods. The design of ANN is assessed by using a feed-forward network based on back propagation delay for getting better optimal solutions under both balanced and unbalanced conditions while the design of ANFIS is based on the adaptive control and state space control strategy. Here sensor less control of DFIG is validated on Simulink with the different techniques like IWO, ANFIS, ANN, and other existing methods [17], [20].

The performance parameters like settling time and peak overshoot of the sensor less speed have been improved a lot with IWO in comparison to AN-FIS, ANN, and other existing methods for balanced conditions and similarly for unbalanced conditions, the least THD is also attained with IWO. The representation of power flow direction in DFIG is shown in Fig.1.

In Fig. 1, the rotor extracts the real power and reactive power from the grid via GSC & RSC. The GSC is uncontrolled and RSC is controlled in nature. The controlling of GSC is done by optimal controllers like IWO, ANFIS & ANN. The stator delivers the real power and reactive power back to the grid. This paper splits into different sections as section II consists of the modeling of DFIG, section III consists of sensor less mode of operation, section IV comprises of the design of ANN structure, and section V deals with the design of ANFIS Structure for converter controlling, section VI consists of design of IWO, section VII discusses the performance assessment with different techniques under balanced and unbalanced condition followed by section VIII i.e., conclusion.

II. MODELING OF DFIG

Let $V_{s\alpha}, V_{s\beta}, V_{r\alpha}, V_{r\beta}$ are the voltages and $I_{s\alpha}, I_{s\beta}, I_{r\alpha}, I_{r\beta}$ are the currents in stationary reference frame coordinates while $V_{sD}, V_{sQ}, V_{rD}, V_{rQ}$ are the voltages and $I_{sD}, I_{sQ}, I_{rD}, I_{rQ}$ are the currents in rotor reference frame coordinates of DFIG. The mathematical modeling of DFIG in stationary reference frame coordinates $(\alpha - \beta)$ is given in terms of stator voltage, stator current, rotor voltage and rotor current are shown from (1) to (4) which are referred from [18],

$$V_{s\alpha} = R_s I_{s\alpha} + L_s \frac{dI_{s\alpha}}{dt} + L_m \frac{dI_{r\alpha}}{dt} \tag{1}$$

$$V_{s\beta} = R_s I_{s\beta} + L_s \frac{dI_{s\beta}}{dt} + L_m \frac{dI_{r\beta}}{dt} \quad (2)$$

$$V_{r\alpha} = \omega_r L_m I_{s\beta} + L_m \frac{dI_{s\alpha}}{dt} + \omega_r L_r I_{r\beta} + R_r I_{r\alpha} + L_r \frac{dI_{r\alpha}}{dt} \quad (3)$$

$$V_{r\beta} = L_m \frac{dI_{s\beta}}{dt} - \omega_r L_m I_{s\alpha} + R_r I_{r\beta} + L_r \frac{dI_{r\beta}}{dt} - \omega_r L_r I_{r\alpha} \quad (4)$$

The modeling equations of DFIG in rotor reference frame coordinates $(D-Q)$ are shown from (5) to (8),

$$V_{sD} = -\omega_r L_s I_{sQ} + R_s I_{sD} + L_s \frac{dI_{sD}}{dt} - \omega_r L_m I_{rQ} + L_m \frac{dI_{rD}}{dt} \quad (5)$$

$$V_{sQ} = R_s I_{sQ} + L_s \frac{dI_{sQ}}{dt} + L_m \frac{dI_{rQ}}{dt} + \omega_r L_m I_{rD} + \omega_r L_s I_{sD} \quad (6)$$

$$V_{rD} = L_m \frac{dI_{sD}}{dt} + R_r I_{rD} + L_r \frac{dI_{rD}}{dt} \quad (7)$$

$$V_{rQ} = L_m \frac{dI_{sQ}}{dt} + R_r I_{rQ} + L_r \frac{dI_{rQ}}{dt} \quad (8)$$

Speed (W_r) can be calculated using (9) which is referred from [19]

$$(T_e - T_L) = BW_r + J\frac{d(W_r)}{dt} \quad (9)$$

where, T_L = Load torque, B = Damping constant, J = inertia constant, T_e = Electromagnetic Torque. On solving linear differential equation as shown in (9), speed can be obtained.

Once the modeling of DFIG has been designed then it is required to consider the effect of the wind turbine system. The wind turbine is used to drive the DFIG. The design aspect of a wind turbine is being directly taken from [18], [19].

III. SENSOR LESS MODE OF OPERATION

It is the process of estimating the rotor position and rotor speed using the current signal only without the involvement of the speed sensor. The advantage of using sensor less operation over the conventional method is that problems like vibration and shaft torsion that occur at the rotor shaft will not be affected on speed measurement because speed is measured from the current signal only.

Initially, rotor current is split into different reference frame coordinates like synchronous, stationary, and rotating reference frames which are shown in Fig. 2. The complete analysis of estimating sensor less speed is shown in the text [17]. By referring Fig. 2, the angle θ_1 (angle between reference rotor current and rotor current in stationary coordinates) is obtained as,

$$\tan(\theta_1) = \frac{i_{r\alpha}}{i_{r\beta}} \quad (10)$$

The angle θ_2 (angle between reference rotor current and rotor current in rotating coordinates) is obtained as shown in (11)

$$\tan(\theta_2) = \frac{i_{rD}}{i_{rQ}} \quad (11)$$

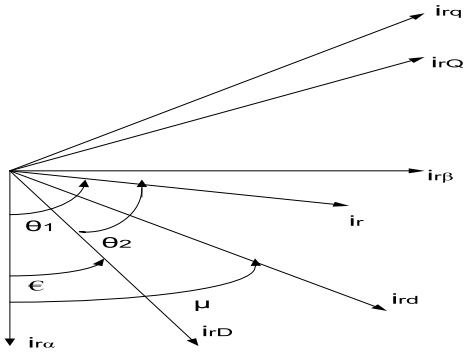

FIGURE 2. Rotor current in different reference frame coordinates [17].

where, $i_{r\alpha}, i_{r\beta}, i_{rD}, i_{rQ}$ are rotor currents in stationary coordinates $(\alpha\text{-}\beta)$, rotating reference frame coordinates $(D-Q)$.

From the Fig. 2 Rotor position $(\varepsilon)$is estimated as shown in (12),

$$\varepsilon = \theta_1 - \theta_2 \quad (12)$$

$$w_{rs} = \mathrm{Cos}(\varepsilon)\frac{d(\mathrm{Sin}(\varepsilon))}{dt} - \mathrm{Sin}(\varepsilon)\frac{d(\mathrm{Cos}(\varepsilon))}{dt} \quad (13)$$

Equation (13) represents the sensor less speed that is obtained by differentiating the rotor position. The equations from (1)-(13) are referred from [17], [18], [19] and these expressions are extended and realized by using various soft computing techniques. The sensor less speed is further realized and controlled by soft computing techniques like ANN, AN-FIS & IWO. Normally, DFIG consists of two back-to-back converters which are mentioned as

A. ROTOR SIDE CONVERTER

Three-phase rotor currents are taken from the brush terminal. Thereafter by using Clarke transformation, 3-phase rotor currents are converted into the stationary reference frame coordinates $(\alpha,\ \beta)$. Further by using park transformation, stationary reference frame coordinates are converted into rotating reference frame (DQ) coordinates as shown in Fig. 2. RSC is a controlled converter that is controlled by using different techniques like IWO, ANFIS, and ANN.

B. GRID SIDE CONVERTER

It is an uncontrolled switch that converts AC to DC directly without any involvement of Gate pulses.

IV. DESIGN OF ARTIFICIAL NEURAL NETWORK (ANN) TOPOLOGY FOR SENSOR LESS SCHEME

There was a certain problem associated with the conventional method for measuring the rotor position and speed under sensor less mode of operation like more overshoot, more settling time, and more THD. To overcome the above problem, ANN topology is used to improve the performance parameters. There are many existing techniques like deep-stacked autoencoder, convolution neural network, and deep belief network for designing the ANN controller. But the feed-forward method using back propagation delay gives the

best results among all for the estimation of sensor less speed, and rotor position which is highly immune to the change in internal parameters. As a result of which the ANN controller is designed by using feed-forward method using back propagation delay. From the concept of partial differentiation, rotor position can be expressed as in (14),

$$d(\varepsilon) = \frac{\partial(\varepsilon)}{\partial\theta_1} d(\theta_1) + \frac{\partial(\varepsilon)}{\partial\theta_2} d(\theta_2) \tag{14}$$

A mathematical expression is required to compute the rotor position by taking tan on both sides in (12),

$$\tan(\varepsilon) = \tan(\theta_1 - \theta_2) \tag{15}$$

After adjusting the terms in (15),

$$\tan(\varepsilon) = \frac{\tan(\theta_1) - \tan(\theta_2)}{1 + \tan(\theta_1)\tan(\theta_2)} \tag{16}$$

Differentiate on both sides with respect to θ_1,

$$\mathrm{Sec}^2(\varepsilon)\frac{d(\varepsilon)}{d(\theta_1)} = \frac{\mathrm{Sec}^2(\theta_1)\mathrm{Sec}^2(\theta_2)}{(1 + \tan(\theta_1)\tan(\theta_2))^2} \tag{17}$$

Differentiate (12) with respect to θ_1,

$$\frac{d(\varepsilon)}{d(\theta_1)} = 1 \tag{18}$$

In the same way, (19) is attained by differentiating the (12) with respect toθ_2,

$$\frac{d(\varepsilon)}{d(\theta_2)} = -1 \tag{19}$$

After putting the values of (18) and (19) in (14),

$$d(\varepsilon) = d(\theta_1) - d(\theta_2) \tag{20}$$

Further integrate (20),

$$\varepsilon = \theta_1 - \theta_2 + b \tag{21}$$

where b is constant of indefinite integration.

After rearranging (10) and (11),

$$\theta_1 = \tan^{-1}(\frac{i_{r\alpha}}{i_{r\beta}}) \tag{22}$$

$$\theta_2 = \tan^{-1}(\frac{i_{rD}}{i_{rQ}}) \tag{23}$$

After putting the values of (23) and (22) in (21),

$$\varepsilon = \tan^{-1}(\frac{i_{r\alpha}}{i_{r\beta}}) - \tan^{-1}(\frac{i_{rD}}{i_{rQ}}) + b \tag{24}$$

Equation (24) can be represented as a basic expression of ANN as shown in (25) & its realization as the basic structure of ANN is shown in Fig. 3,

$$\varepsilon = W_1X_1 + W_2X_2 + b \tag{25}$$

where, $X_1$and X_2 are the inputs of ANN,

$$X_1 = 1, \quad X_2 = -1 \tag{26}$$

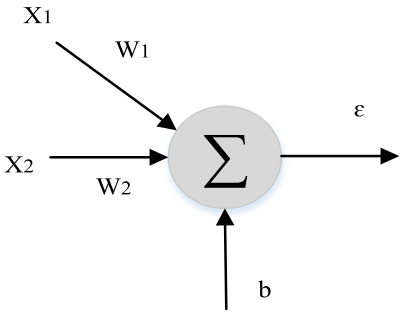

FIGURE 3. Structure of neural network.

TABLE 1. Weight used in ANN and bias.

Parameters	Value
X_1	1
X_2	-1
W_1	53
W_2	87
b	2.7

where, $W_1$and W_2 are the inputs of ANN,

$$W_1 = \tan^{-1}(\frac{i_{r\alpha}}{i_{r\beta}}), \quad W_2 = \tan^{-1}(\frac{i_{rD}}{i_{rQ}}) \tag{27}$$

b and ε are the bias and output in Fig. 3.

Actual output is sigmoid in nature which is given by,

$$Act(\varepsilon) = \frac{1}{(1 + e^{-\varepsilon})} \tag{28}$$

Since the value of X_1 and X_2 are constant while W_1 and W_2 are calculated from (27) & its value is also shown in Table 1. The difference between the estimated and reference value of output (ε) is causing an error which is estimated by using Steepest Descent Algorithm,

$$E = \frac{(\varepsilon - \varepsilon_{(ref)})^2}{2} \tag{29}$$

The error will be used as feedback to adjust the different weights based on back propagation delay for getting the desired output which is discussed in a subsequent manner. The back propagation delay is simply used as feedback to improve the performance of the output. The error produced in (29) will be updated the weights (W) by using the steepest descent algorithm,

$$W_j(new) = W_j(old) - \eta\frac{\partial(E)}{\partial W_j} \tag{30}$$

where, η is learning rate, $0 < \eta < 1$, $\eta = 0.5$

In (30), the derivative of the error with respect to weight can also be split into different components,

$$\frac{\partial(E)}{\partial W_j} = \frac{\partial(E)}{\partial\varepsilon} * \frac{\partial(\varepsilon)}{\partial Act(\varepsilon)} * \frac{\partial Act(\varepsilon)}{\partial W_j} \tag{31}$$

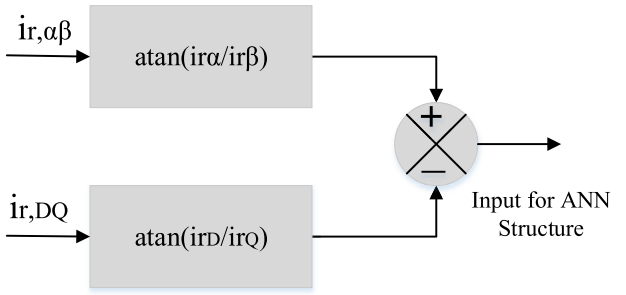

FIGURE 4. Selection of inputs signals for ANN.

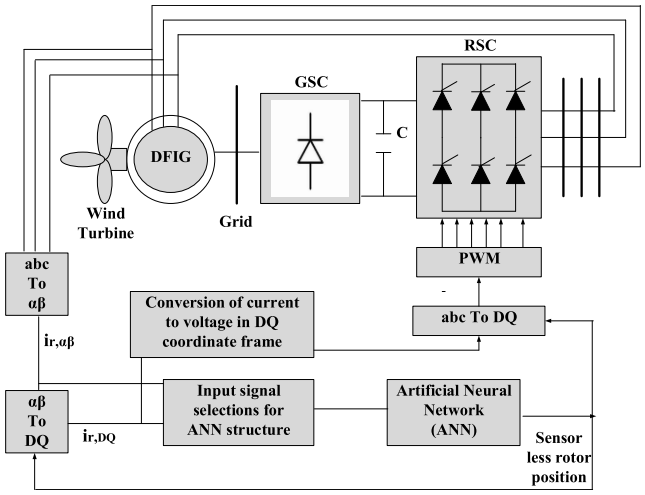

FIGURE 5. Structure of sensor less based DFIG using artificial neural network.

On differentiating (29),

$$\frac{\partial(E)}{\partial \varepsilon} = (\varepsilon - \varepsilon_{(ref)}) \tag{32}$$

On differentiating (28),

$$\frac{\partial(\varepsilon)}{\partial Act(\varepsilon)} = -\frac{(1+e^{-\varepsilon})^2}{e^{-\varepsilon}} \tag{33}$$

Further differentiate (25),

$$\frac{\partial Act(\varepsilon)}{\partial W_j} = X_j \tag{34}$$

After putting the values of (32), (33), and (34) in (31),

$$\frac{\partial(E)}{\partial W_j} = -\frac{(1+e^{-\varepsilon})^2}{e^{-\varepsilon}} * (\varepsilon - \varepsilon_{(ref)}) * X_j \tag{35}$$

where, $\eta = 0.75$

The upgraded weights are shown in Table 2. The rotor current in rotating reference frame (DQ) coordinates along with stationary reference frame coordinates (α, β) will give an input signal to the ANN structure as shown in Fig. 4.

By referring to Fig. 5, The output of the ANN gives sensor less rotor position which acts as a catalyst for the generation of the reference voltage for the PWM signal which further gives switching pulses for the RSC converter.

TABLE 2. Upgraded weights & bias in ANN.

Parameters	Value
W_1	82.98
W_2	68.98
b	5.9

A similar kind of converter controlling based on ANN can also be assessed for unbalancing conditions like three-phase fault, the line to ground fault, line to line fault, and double line to ground fault & such realization can also be observed in Fig. 6.

After the up-gradation of weights for the sensor less speed controlling, the performance of sensor less speed and rotor position is improved a lot with back propagation delay. The value of the upgraded weights is shown in Table 2. Still, there is a scope of improvement of performance parameters that will be overcome by another technique ANFIS which is discussed in the next section.

V. DESIGN OF ANFIS FOR CONVERTER CONTROLLING OF DFIG BASED ON SENSOR LESS OPERATION

The design of the ANFIS for the converter controlling of DFIG of the sensor less scheme is based on two aspects which are discussed in this section.

A. STATE SPACE MODEL OF DFIG USING SENSOR LESS MODE OF OPERATION

The state-space model of DFIG will be analyzed in both the stationary reference frame & rotor reference frame. It begins with the modeling of DFIG in the stationary reference frame. The state-space modeling of DFIG begins from (1) to (4) in which rotor currents in the stationary coordinate (α) are substituted in terms of the stationary coordinate (β)by using the (10). The modified equations after such substitution are represented from (36) to (39) which are given as,

$$V_{s\alpha} = R_s I_{s\alpha} + L_s \frac{dI_{s\alpha}}{dt} + L_m \frac{d(I_{r\beta}\tan(\theta_1))}{dt} \tag{36}$$

$$V_{s\beta} = R_s I_{s\beta} + L_s \frac{dI_{s\beta}}{dt} + L_m \frac{dI_{r\beta}}{dt} \tag{37}$$

$$V_{r\alpha} = \omega_r L_m I_{s\beta} + L_m \frac{dI_{s\alpha}}{dt} + \omega_r L_r I_{r\beta} + R_r I_{r\alpha} + L_r \frac{dI_{r\alpha}}{dt} \tag{38}$$

$$V_{r\beta} = L_m \frac{dI_{s\beta}}{dt} - \omega_r L_m I_{s\alpha} + R_r I_{r\beta} + L_r \frac{dI_{r\beta}}{dt} - \omega_r L_r I_{r\beta}\tan(\theta_1) \tag{39}$$

The general representation of state-space model of DFIG in stationary reference coordinates is represented with the help of a block diagram as shown in Fig. 7. In this block diagram, input is $V_{\alpha\beta}$ and the output is $I_{\alpha\beta}$. The standard mathematical representation of state space equation is,

$$\dot{I}_{\alpha\beta} = A \cdot I_{\alpha\beta} + B \cdot V_{\alpha\beta}$$
$$\overset{\Delta}{\dot{I}}_{\alpha\beta} = C \cdot I_{\alpha\beta} \tag{40}$$

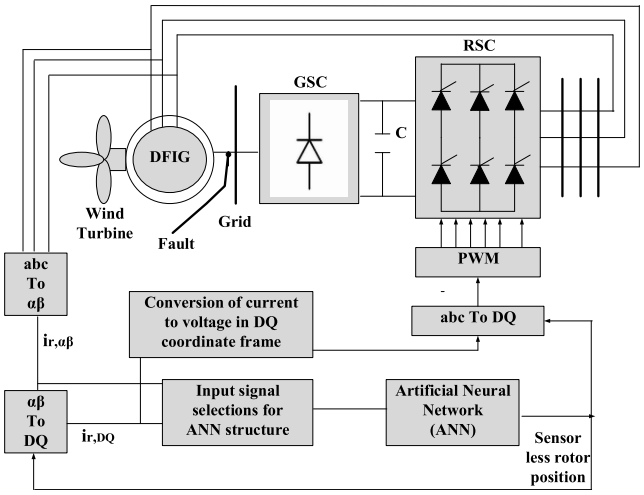

FIGURE 6. Fault Analysis of DFIG using Artificial neural network.

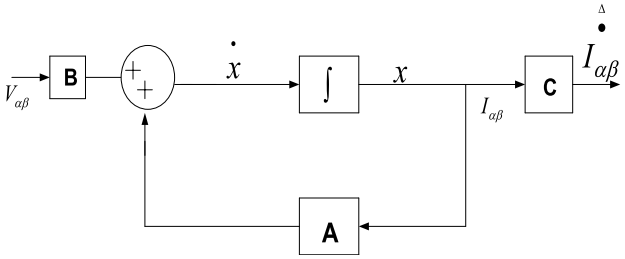

FIGURE 7. Generalized State space representation of DFIG in stationary reference frame.

where,

$$\dot{I}_{\alpha\beta} = \begin{bmatrix} \dot{I}_{s\alpha} \\ \dot{I}_{s\beta} \\ \dot{I}_{r\alpha} \\ \dot{I}_{r\beta} \end{bmatrix}, \quad I_{\alpha\beta} = \begin{bmatrix} I_{s\alpha} \\ I_{s\beta} \\ I_{r\alpha} \\ I_{r\beta} \end{bmatrix}, \quad V_{\alpha\beta} = \begin{bmatrix} V_{s\alpha} \\ V_{s\beta} \\ V_{r\alpha} \\ V_{r\beta} \end{bmatrix}$$

$$A = \begin{bmatrix} \frac{-R_s}{L_s} & 0 & 0 & \frac{-L_m \tan(\theta_1)p}{L_s} \\ 0 & \frac{-R_s}{L_s} & 0 & \frac{-L_m}{L_s} \\ \frac{-L_m p}{L_r} & \frac{-\omega_r L_m}{L_r} & \frac{-R_r}{L_r} & \frac{-\omega_r L_r}{L_r} \\ \frac{\omega_r L_m}{L_r} & \frac{-L_m p}{L_r} & 0 & \frac{-R_r + \omega_r L_r \tan(\theta_1)}{L_r} \end{bmatrix},$$

$$p = \frac{d}{dt}$$

$$B = \begin{bmatrix} \frac{1}{L_s} & 0 & 0 & 0 \\ 0 & \frac{1}{L_s} & 0 & 0 \\ 0 & 0 & \frac{1}{L_r} & 0 \\ 0 & 0 & 0 & \frac{1}{L_r} \end{bmatrix}$$

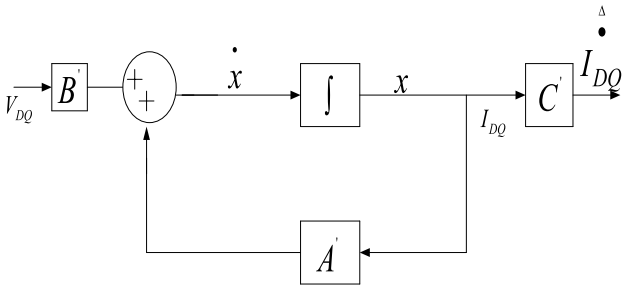

FIGURE 8. Generalized State space representation of DFIG in rotor reference frame.

Such state space model of DFIG can also be realized as adaptive model if accurate value of $(\theta_1, \theta_2)$are known then matrix A will be changed to $\overset{\Delta}{A}$. Now (40) will be modified as,

$$\dot{\overset{\Delta}{I}}_{\alpha\beta} = \overset{\Delta}{A} \cdot \overset{\Delta}{I}_{\alpha\beta} + B \cdot V_{\alpha\beta} \tag{41}$$

Now the modeling of DFIG is analyzed in the rotor reference frame by using state-space model. Substitute value of (11) in the expressions from (5) to (8) & modified expressions are shown from (42) to (45) as,

$$V_{sD} = -\omega_r L_s I_{sQ} + R_s I_{sD} + L_s \frac{dI_{sD}}{dt} - \omega_r L_m I_{rQ} + L_m \frac{d(\tan(\theta_2) I_{rQ})}{dt} \tag{42}$$

$$V_{sQ} = R_s I_{sQ} + L_s \frac{dI_{sQ}}{dt} + L_m \frac{dI_{rQ}}{dt} + \omega_r L_m \tan(\theta_2) I_{rQ} + \omega_r L_s I_{sD} \tag{43}$$

$$V_{rD} = L_m \frac{dI_{sD}}{dt} + R_r I_{rD} + L_r \frac{dI_{rD}}{dt} \tag{44}$$

$$V_{rQ} = L_m \frac{dI_{sQ}}{dt} + R_r I_{rQ} + L_r \frac{dI_{rQ}}{dt} \tag{45}$$

The general representation of state space model of DFIG in rotor reference frame coordinates is represented by a block diagram as shown in Fig. 8. In this block diagram, input is V_{DQ} and output is I_{DQ}. The mathematical expression of state space equations in the rotor reference frame is,

$$\dot{I}_{DQ} = A' \cdot I_{DQ} + B' \cdot V_{DQ} \tag{46}$$

$$\dot{\overset{\Delta}{I}}_{DQ} = C' \cdot I_{DQ} \tag{47}$$

where,

$$A' = \begin{bmatrix} \frac{-R_s}{L_s} & \frac{-\omega_r L_s}{L_s} & 0 & \frac{-p\tan(\theta_2)L_m + \omega_r L_m}{L_s} \\ \frac{-\omega_r L_s}{L_s} & \frac{-R_s - pL_s}{L_s} & 0 & \frac{-pL_m - \omega_r L_m \tan(\theta_2)}{L_s} \\ \frac{-pL_m}{L_r} & 0 & \frac{-R_r}{L_r} & 0 \\ 0 & \frac{-pL_m}{L_r} & 0 & \frac{-R_r}{L_r} \end{bmatrix},$$

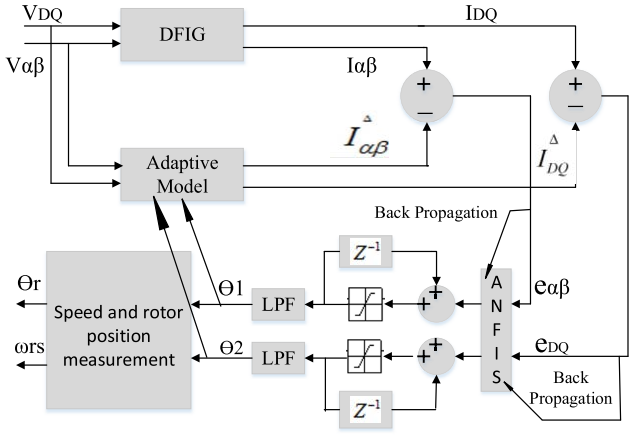

FIGURE 9. Block diagram of ANFIS based speed & position estimation.

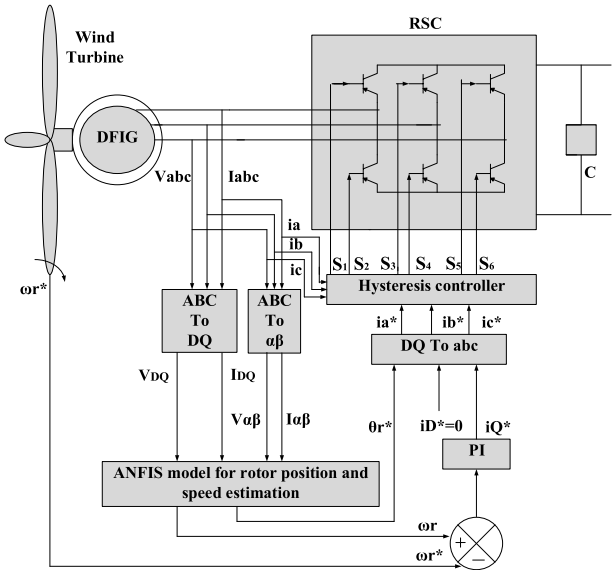

FIGURE 10. Control stragedy diagram of proposed system.

$$p = \frac{d}{dt}$$

$$B' = \begin{bmatrix} \frac{1}{L_s} & 0 & 0 & 0 \\ 0 & \frac{1}{L_s} & 0 & 0 \\ 0 & 0 & \frac{1}{L_r} & 0 \\ 0 & 0 & 0 & \frac{1}{L_r} \end{bmatrix}$$

$C \& C'$ are taken from adaptive model in order to get desired output.

B. ARCHITECTURE OF ANFIS BASED DFIG USING SENSOR LESS MODE OF OPERATION

The structure of ANFIS for estimating the sensor less speed & rotor position of DFIG is shown in Fig. 9 along with the control stragedy in Fig. 10. In this structure, an adaptive model

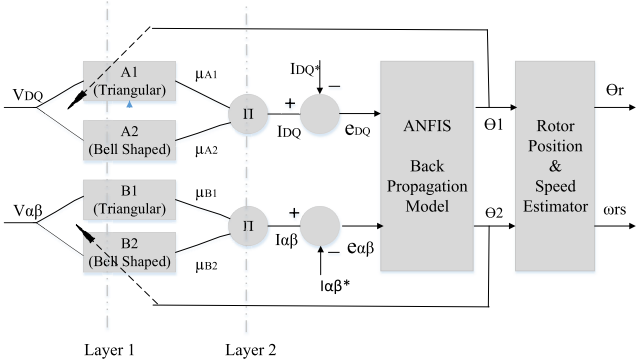

FIGURE 11. Schematic representation of ANFIS architecture.

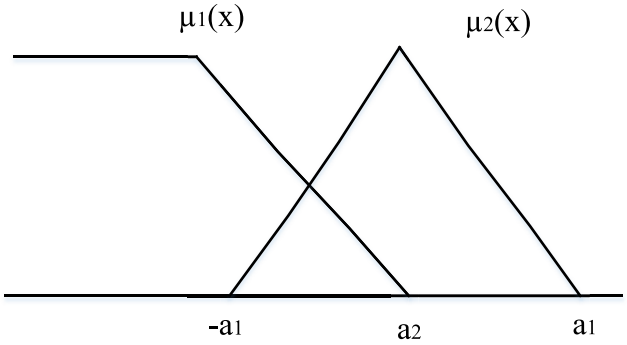

FIGURE 12. Fuzzy membership functions.

is designed & trained in order to give the desired output. The inputs to ANFIS structure are e_{DQ} & $e_{\alpha\beta}$ while the outputs are θ_1 & θ_2 which are obtained after passing through low pass filter (LPF). The inputs to the ANFIS are being taken by considering the difference between voltage in stationary and rotating reference frame coordinates. The output of ANFIS is further used to train the adaptive controller by using back propagation delay. The schematic structure of ANFIS with the help of propagation delay is shown in Fig. 11. Such schematic structure consists of two layers. These two layers are discussed here.

LAYER 1: It consists of 4 nodes which are represented by the square as shown in Fig. 11. The membership function for corresponding nodes is represented in form of triangle & trapezoidal nodes as shown in Fig. 12. The mathematical representation of the membership function is shown in (48) and (49).

$$\mu_{A1} = \mu_{B1} = \begin{cases} 1, & X \le -a_1 \\ \dfrac{X - a_2}{-a_1 - a_2}, & -a_1 < X < a_2 \\ 0, & X > a_2 \end{cases} \tag{48}$$

$$\mu_{A2} = \mu_{B2} = \begin{cases} 1 - \dfrac{X - a_2}{a_1}, & |X - a_2| \le a_1 \\ 0, & |X - a_2| \ge a_1 \end{cases} \tag{49}$$

where the value of a_1, a_2 is adjusting according to error.

LAYER 2: The outputs of layer 2 are,

$$I_{DQ} = \mu_{A1}\mu_{A2} \tag{50}$$

$$I_{\alpha\beta} = \mu_{B1}\mu_{B2} \tag{51}$$

The switching model is shown in Fig. 11 in which the inputs of the ANFIS structure are errors in stationery and reference frame coordinates which generates output $\theta_1 \& \theta_2$. Further, these angles will generate rotor position and sensor less speed.

C. ANFIS TRAINING STRUCTURE

Refer to Fig. 11, three-phase voltages and three-phase currents are measured from the stator terminal and further transformed into a stationary reference frame and rotating reference frames with the set of membership functions of ANFIS as discussed in the previous section. After that, these transformed currents are used to generate the error in the rotating reference frame as,

$$e_{DQ} = I_{DQ} - I^*_{DQ} \tag{52}$$

In the same way, these transformed currents are used to generate the error in the stationary reference frame as,

$$e_{\alpha\beta} = I_{\alpha\beta} - I^*_{\alpha\beta} \tag{53}$$

The exact relationship between input and output of ANFIS is realized as,

$$\theta_1 = e_{DQ}\ln(e_{\alpha\beta}) + e_{\alpha\beta}\ln(e_{DQ}) \tag{54}$$

$$\theta_2 = e_{DQ}\ln(e_{\alpha\beta}) - e_{\alpha\beta}\ln(e_{DQ}) \tag{55}$$

Further (54) & (55) are expressed in the standard form of ANN,

$$\theta_1 = e_{DQ}W_1 + e_{\alpha\beta}W_2 \tag{56}$$

$$\theta_2 = e_{DQ}W_1 - e_{\alpha\beta}W_2 \tag{57}$$

where,

$$W_1 = \ln(I_{\alpha\beta} - I^*_{\alpha\beta}) \tag{58}$$

$$W_2 = \ln(I_{DQ} - I^*_{DQ}) \tag{59}$$

The symbolic representation of weights is shown in (58) and (59). With the help of back propagation delay, weights are trained by using steepest descent algorithm as shown in (60).

$$W_K(new) = W_K(old) - \eta\frac{\partial(E)}{\partial W_K} \tag{60}$$

where actual error is,

$$E = \frac{(\theta - \theta_{ref})^2}{2} \tag{61}$$

where, $k = 1, 2 \& \theta = \theta_1 - \theta_2, \eta = 0.5$

Last term of the (60) can be expanded as,

$$\frac{\partial(E)}{\partial W_k} = \frac{\partial(E)}{\partial I_{D,Q}}\frac{\partial(I_{D,Q})}{\partial I_{\alpha,\beta}}\frac{\partial(I_{\alpha,\beta})}{\partial W_k} \tag{62}$$

From (52) to (62), the design of ANFIS structure is represented which helps to analyze the performance parameters. In a similar way, the control strategy of the proposed network is shown in Fig. 10. In this voltage and current of rotating reference frame coordinates produces the measured speed which is further compared with its reference value and this change in speed passes through the PI controller ($Kp = 36.9, Ki = 9.8$) for the generation of quadrature axis current (i_q) keeping direct axis current ($i_d = 0$). Further d-q current is converted into three-phase current which helps to generate the reference voltage for the PWM signal for the generation of pulse for the hysteresis controller. In a similar way, voltage and current of stationary reference frame coordinates produce rotor position and which further converts d-q into three-phase signals.

VI. DESIGN OF INVASE WEED OPTIMIZATION (IWO)

A.R. Mehrabian was the one who came up with the idea of IWO. The invasive weed meta-heuristic algorithm is a population-based optimization technique that finds the general optimum solution of a mathematical function by imitating the compatibility and randomness of a weed colony. Weeds are tough plants with a proclivity for spreading a serious threat to crops. As a result of these features, they have proven to be exceptionally durable and adaptable to changes in the world resulting in an effective optimization method. Tolerance, adaptability, and unpredictability are all features that the program aims to replicate in a weed group survey. Colonies of invasive weed is a phenomenon in agriculture that is highly inspired by this strategy. A weed is a plant that grows inadvertently, according to a common definition. While weeds may have numerous uses and benefits in some areas, it is considered weeds because it develops in an area that interferes with human requirements and activities. The ''Invasive Weed Optimization Technique'' has been presented as a simple numerical optimization algorithm that is based on colonized weed. Using basic properties such as seeding, development, and competition in a weed colony, this algorithm is simple but successful in convergent to optimal solutions. The process of IWO is explained through a flowchart as shown in Fig. 13.

The brief design of the flowchart showing the IWO algorithm is explained through the following steps:

1) Population initialization is defined as a dispersed number of seeds in the space available.
2) Reproduction is the process through which each seed develops into a flowering plant and generates seeds that are dependent on their fitness value. The number of grains or seeds of grasses (s) decreases linearly from $S_{\max}$ to $S_{\min}$ and is given as,

$$S = \frac{f_i - f_{worst}}{f_{best} - f_{worst}}(S_{\max} - S_{\min}) + S_{\min} \tag{63}$$

where, $S_{\max}$ and $S_{\min}$ are the maximum and minimum number of seeds respectively, f_{best} and f_{worst} are the best and worst objective function value respectively. f_i is the fitness function which is the fault current in this case. The seeds generated by the group with the

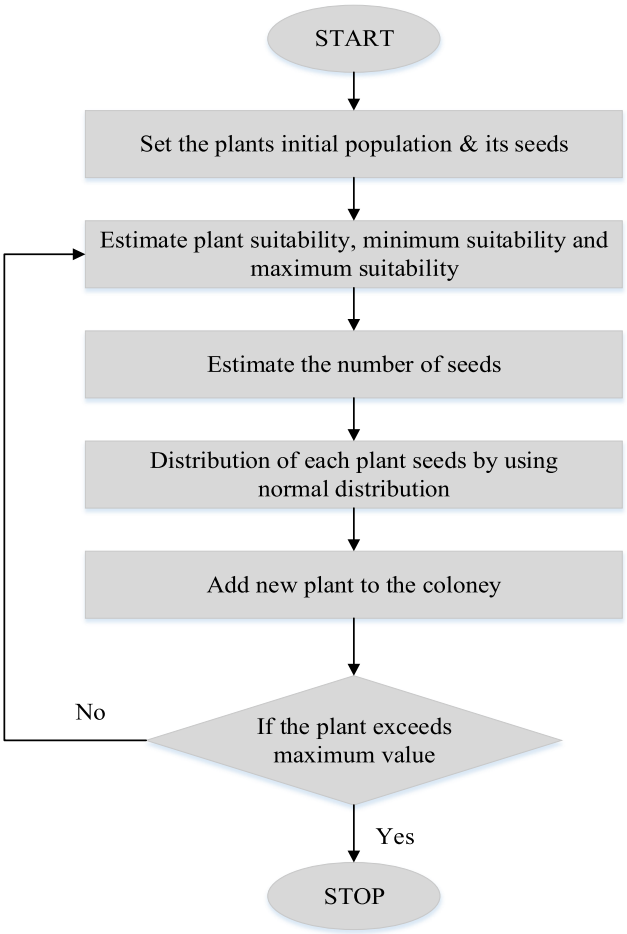

FIGURE 13. Flowchart explaining the IWO mechanism.

average planting location and standard deviation in a normal distribution (σ)are produced as,

$$\sigma = \left(\frac{r_{\max} - r}{r_{\max}}\right)^{n} (\sigma_{initial} - \sigma_{final}) + \sigma_{final} \quad (64)$$

where $r_{\max}$ is the number of maximum iterations, σ is the current standard deviation, n is the nonlinear modulation index, $\sigma_{initial}$ and σ_{final} are initial and final values of standard deviation respectively.

VII. PERFORMANCE ASSESSMENT ON DIFFERENT TECHNIQUES

The performance assessment of sensor less control has been analyzed for both balanced and unbalanced conditions.

A. PROPOSED TOPOLOGY VALIDATION WITH BALANCED CONDITION

The design aspects of sensor less speed control of DFIG with different techniques like IWO, ANFIS & ANN are already discussed in Sections VI, V, and IV.

Further, the design topology based on different techniques is being performed on Simulink. The performance assessment for sensor less control is being assessed at no load, half load, and full load. It is observed that the sensor less speed and torque of DFIG at full load settled faster with less peak overshoot under the technique IWO in comparison to

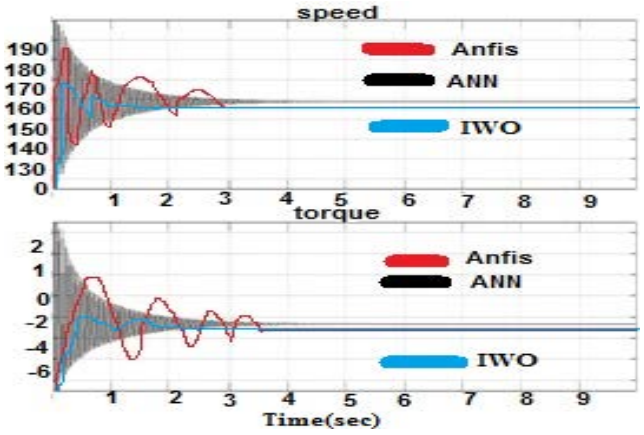

FIGURE 14. Sensor less speed & Torque of DFIG with different techniques under full load.

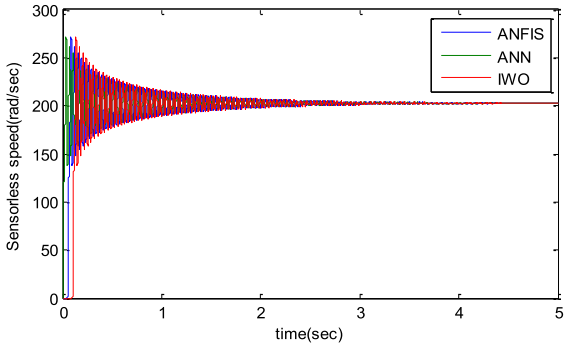

FIGURE 15. Sensor less speed of DFIG with different techniques under no load.

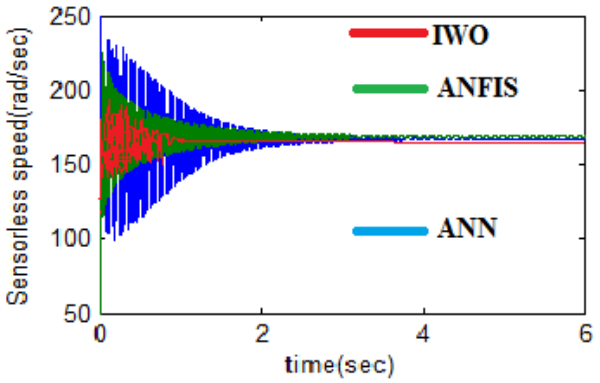

FIGURE 16. Sensor less speed of DFIG with different techniques under half load.

TABLE 3. Comparative analysis of peak overshoot for sensor less speed with different technique.

Peak Overshoot (%)	IWO	ANFIS	ANN	Ref. [17]	Ref. [20]
No load	4.51	5.68	6.84	7.12	7.25
half load	3.99	4.86	5.84	6.98	7.02
full load	4.56	5.56	6.89	7.11	7.89

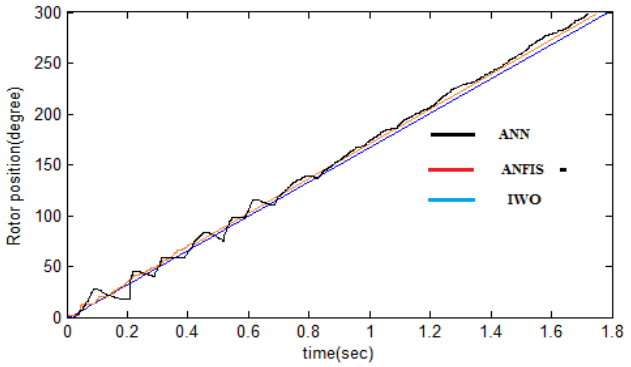

FIGURE 17. Rotor position of DFIG with different techniques under full load.

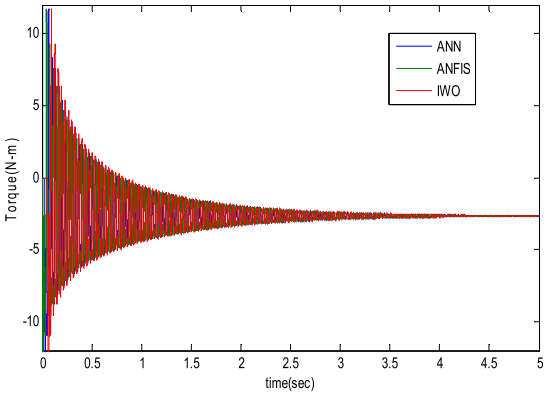

FIGURE 18. Torque of DFIG with different techniques under no load.

TABLE 4. Comparative analysis of settling time for sensor less speed with different technique.

Settling time (sec)	IWO	ANFIS	ANN	Ref. [17]	Ref. [20]
No load	2.4	3	4.1	6.35	6.58
half load	2.9	3.5	4	5.98	6.12
full load	3.1	3.8	4.2	6.11	6.54

ANFIS & ANN as shown in Fig. 14. In this figure, a negative value of torque also assures the generating mode of operation of DFIG. Similar kinds of results are also obtained for sensor less speed at no load and half load as shown in Fig. 15 & Fig. 16. The rotor position of DFIG under full load is also shown in Fig. 17 while torque of DFIG under no load is shown in Fig. 18. The overall comparative analysis in terms of peak overshoot for sensor less speed of DFIG with different techniques is shown in Table 3. It is observed that minimum peak overshoot is obtained with IWO in comparison to ANFIS and ANN under different loading conditions. It also provides improved results in comparison to existing techniques [17], [20] & its graphical aspects are also shown in Fig. 19. In the same way, minimum settling time is obtained with IWO in comparison to ANFIS, ANN, and existing techniques with different loading conditions as

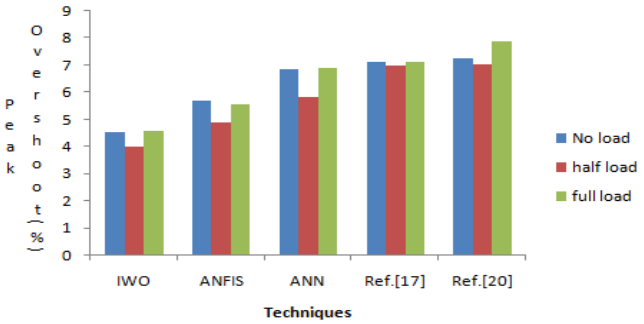

FIGURE 19. Graphical comparative analysis of peak overshoot.

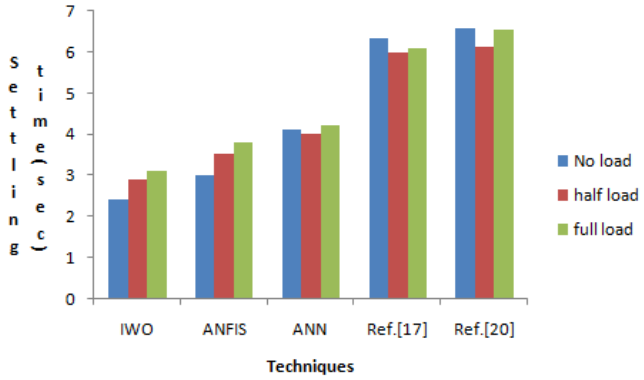

FIGURE 20. Graphical comparative analysis of settling time.

TABLE 5. Comparative analysis of peak overshoot with IWO, ANFIS, ANN and other techniques [25].

Peak Overshoot (%)	IWO	ANFIS	ANN	MRAS [25]	Sensor less stragedy [25]
No load	4.51	5.68	6.84	7.32	7.53
half load	3.99	4.8	5.84	7.22	7.31
full load	4.56	5.56	6.89	8.13	8.56

shown in Table 4. The graphical comparison of settling time with different loading conditions is shown in Fig. 20.

Another comparative analysis for the sensor less speed control of DFIG for the estimation of performance parameters like settling time and peak overshoot are assessed with [25] under balanced condition. In [25], there are two methods discussed named as conventional sensor less stragedy and model reference adaptive system (MRAS). The design aspect of these two methods is already discussed in detail [25] with the same machine rating as given in appendix. The comparative analysis for measurement of peak overshoots of speed sensor less speed with various methods IWO, ANFIS, ANN, and two methods mentioned in [25] is shown in Table 5 and its graphical analysis is represented in Fig. 21.

The comparison of IWO, ANFIS, ANN, and two approaches specified in [25] for measuring the settling time of sensor-less speed is provided in Table 6, and its graphical analysis is depicted in Fig. 21.

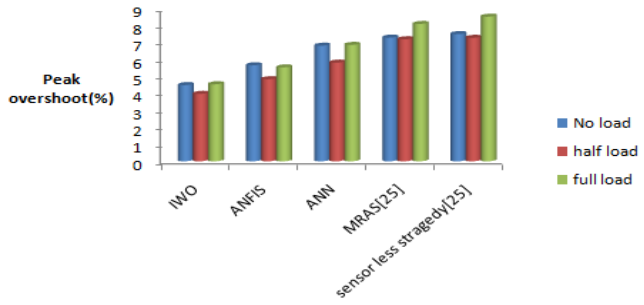

FIGURE 21. Graphical comparative analysis of peak overshoot with IWO, ANFIS, ANN and other techniques [25].

TABLE 6. Comparative analysis of settling time for sensor less speed with IWO, ANFIS, ANN and other different techniques [25].

Settling time (sec)	IWO	ANFIS	ANN	MRAS [25]	Sensor less stragedy [25]
No load	2.4	3	4.1	6.87	7.01
half load	2.9	3.5	4	6.15	6.23
full load	3.1	3.8	4.2	6.68	6.98

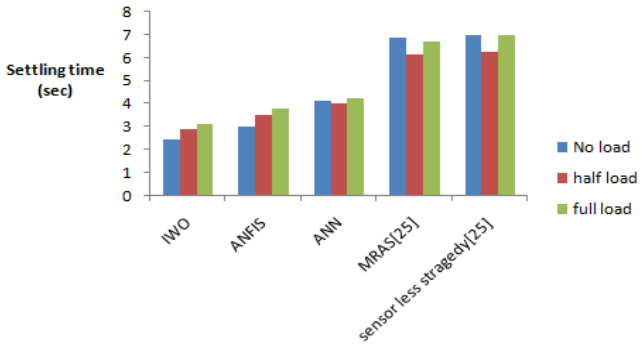

FIGURE 22. Graphical comparative analysis of settling time with IWO, ANFIS, ANN and other techniques [25].

From Table 5, it can be depicted that peak overshoot of the sensor less speed is found to be least with IWO in comparison to ANFIS, ANN, MRAS [25], and sensor less stragedy [25]. Similar kind of analysis is also realized graphically from Fig. 21. Subsequently, Table 6 shows that, in comparison to ANFIS, ANN, MRAS [25], and sensor less stragedy [25], IWO is shown to have the least sensor less speed settling time. Analysis of a similar nature is also visualized graphically in Fig. 22.

B. PERFORMANCE OF DFIG UNDER UNBALANCED CONDITION

In the unbalanced condition, different types of faults like three-phase fault, single line to ground fault, line to line fault, and double line to ground faults occur at the grid terminal as shown in Fig. 6. Performance analysis of DFIG under unbalanced conditions is assessed with different techniques like IWO, ANFIS, and ANN which occur at the grid terminal. The design of the protective scheme to protect the grid-connected

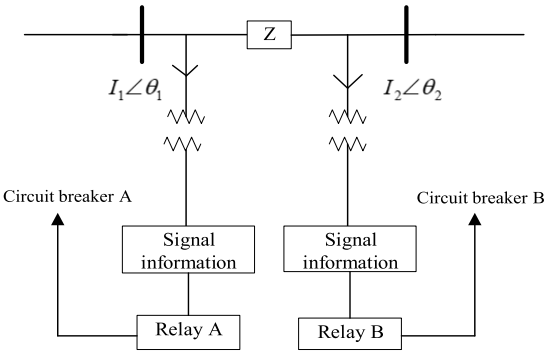

FIGURE 23. Structure of protective scheme for grid integrated DFIG system.

system is assessed by considering the protective elements like circuit breaker and relay as shown in Fig. 22. It begins with the measurements of post fault (I_1) and pre-fault (I_2) current at the grid terminal. Since both these currents are alternating in nature and there will be particular phase angles that exist for both alternate quantities. The currents (I_1) and current (I_2) are used for the protection scheme as one of the input valuable parameters. Before both these currents are chosen for measurement in the protection scheme, these currents have been controlled with the different techniques IWO, ANFIS, and ANN. The design aspects of these methods are already discussed in the previous sections. Once the currents I_1, I_2 are measured from the respective techniques. Now it is required to measure the modulation index $'m'$ as one of the significant parameters for the protective scheme as,

$$m = \frac{I_1\angle\theta_1 - I_2\angle\theta_2}{I_1\angle\theta_1 + I_2\angle\theta_2} \tag{65}$$

where, $\theta_1 = \tan^{-1}(\frac{I_1}{I_2})$, $\theta_2 = \tan^{-1}(\frac{I_2}{I_1})$

The Equation (65) can be extended in further steps by converting the polar form to a rectangular form,

$$m = \frac{(I_1\cos\theta_1 + I_2\cos\theta_2) + j(I_1\sin\theta_1 - I_2\cos\theta_2)}{(I_1\cos\theta_1 + I_2\cos\theta_2) + j(I_1\sin\theta_1 - I_2\cos\theta_2)} \tag{66}$$

Also, the magnitude of (66) can be represented as,

$$|m| = \frac{\sqrt{(I_1\cos\theta_1 + I_2\cos\theta_2)^2 + (I_1\sin\theta_1 - I_2\cos\theta_2)^2}}{\sqrt{(I_1\cos\theta_1 + I_2\cos\theta_2)^2 + (I_1\sin\theta_1 + I_2\cos\theta_2)^2}} \tag{67}$$

The structure of the protective scheme for tripping the fault in the system due to unbalanced conditions is shown in Fig. 23. In the structure, the modulation index (m) is measured and compared with its reference value (m_{index}). If $m > m_{index}$ then the command is given to relay and circuit breaker for tripping the fault otherwise measured value of modulation index is re-adjusted by modifying the post-fault and pre-fault currents with the help of different techniques like IWO, ANFIS, and ANN. The complete process of tripping the faults is also illustrated through a flowchart as shown in Fig. 24.

Algorithm 1 Process of Protective Scheme

Step 1: Estimate index m which is given in (65)
Step 2: Adjust the phase and magnitude in step 1 for m
Step 3: Check the condition of fault tripping by reference index (m_{index})
Step 4: if $m > m_{index}$ command is given to trip the fault
Step 5: if $m < m_{index}$then adjust the estimated modulation index

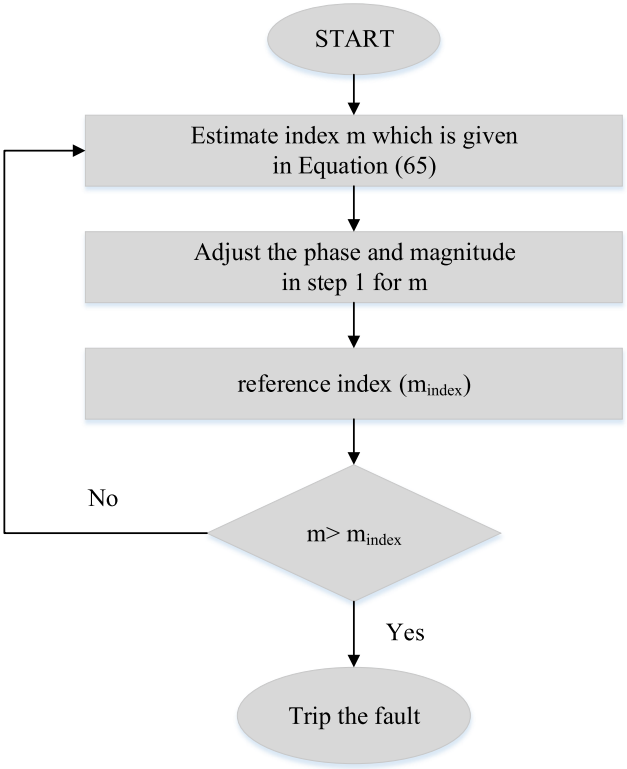

FIGURE 24. Flowchart illustrating the protective structure.

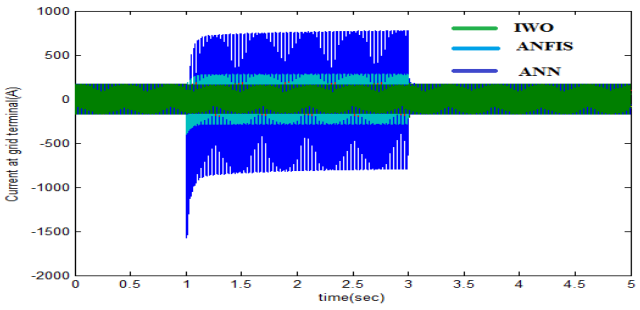

FIGURE 25. Comparative current analysis at grid terminal of DFIG with different techniques under three phase fault.

In the grid integrated system, the stator of the DFIG is directly connected to the grid. It means that if any unbalancing occurs at the grid terminal, then it will directly affect the stator terminal. In order to prevent the system from different kinds of faults, a protective scheme is developed as discussed

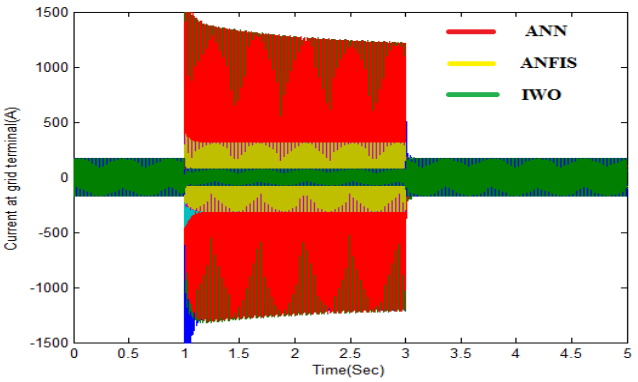

FIGURE 26. Comparative current analysis at grid terminal of DFIG with different techniques under single line to ground fault.

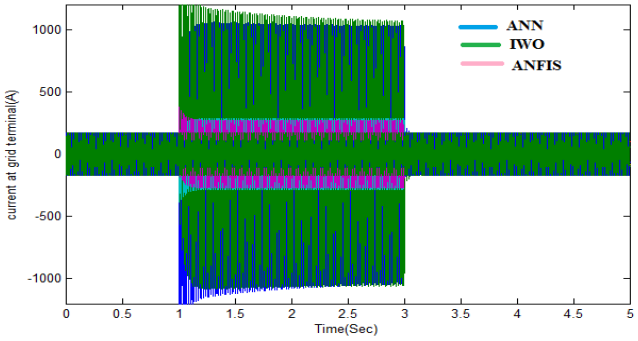

FIGURE 27. Comparative current analysis at grid terminal of DFIG with different techniques under line-to-line fault.

in section VII-B. In the given system, various kinds of faults occur at the grid terminal in the time interval between 1sec to 3sec. The system is found in a healthy state before t=1 sec and after t=3 sec. Further, it is observed that the current in the faulty region trip up to a certain extent and approaches to healthy state quite well with IWO in comparison to ANFIS & ANN for the three-phase fault occurrence at grid terminal for the time interval between t=1 to 3 sec as shown in Fig. 25. The distortion level in terms of THD of the grid current is found to be minimum with IWO in comparison to ANFIS & ANN for three-phase fault. In the same way, faulty current trips with minimum distortion in regaining their original state better with IWO in comparison to ANFIS & ANN for single line to ground fault, line to line fault, and double line to ground fault as shown in Fig. 26, Fig. 27, and Fig. 28. The overall comparative analysis of distortion (THD) with different techniques is shown in Table 7.

The comparative analysis of fault currents distortion which occurs at grid terminal current is analyzed in terms of THD (%) for the different kinds of faults as shown in Table 7. It is observed that minimum THD is attained with IWO in comparison to ANFIS & ANN for all kinds of faults. It is also observed that faulty current approaches the healthy current very closely with the IWO technique in comparison to other techniques. The distortion level (in terms of THD)

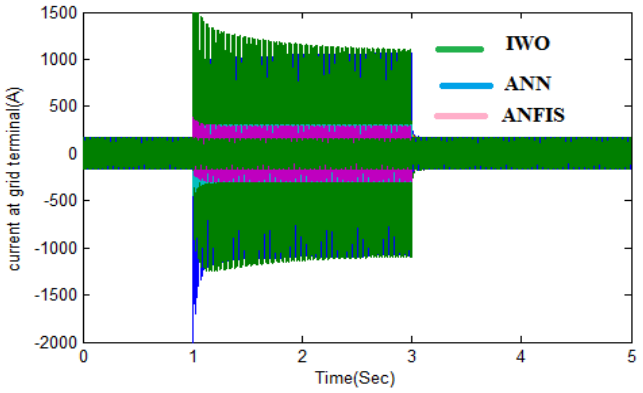

FIGURE 28. Comparative current analysis at grid terminal of DFIG with different techniques under double line to ground fault.

TABLE 7. Comparative THD (%) of grid current with different techniques.

THD (%)	IWO	ANFIS	ANN	Ref. [17]	Ref. [20]
Three phase fault	5.69	6.69	7.12	7.78	8.11
single line to ground fault	5.12	6.11	6.98	7.12	7.99
line to line fault	4.99	5.69	6.32	7.4	7.9
double line to ground fault	5.01	5.84	6.32	6.87	7.12

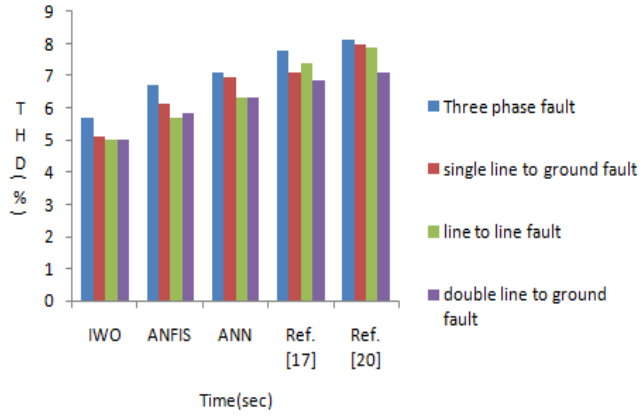

FIGURE 29. Graphical comparative THD (%) of grid current with different techniques

is also found to be minimum with IWO in comparison with ANFIS, ANN & other existing techniques ([17] and [20]). Such analysis proves that IWO shows better results for sensor less speed control with respect to other methods for all types of conditions. A similar kind of comparative performance analysis is also shown graphically as shown in Fig. 29.

The comparative analysis of unbalancing conditions can also be realized with two methods mentioned in [25]. As discussed in the section VII-A, MRAS and sensor less stragedy are the two methods mentioned in [25]. The THD (%) of the grid current are compared with IWO. ANFIS, ANN,

TABLE 8. Comparative THD (%) of grid current with IWO, ANFIS, ANN and other different techniques [25].

THD (%)	IWO	ANFIS	ANN	MRAS [25]	Sensor less stragedy [25]
Three phase fault	5.69	6.69	7.12	8.16	8.36
single line to ground fault	5.12	6.11	6.98	8.16	8.87
line to line fault	4.99	5.69	6.32	8.10	8.61
double line to ground fault	5.01	5.84	6.32	7.32	7.71

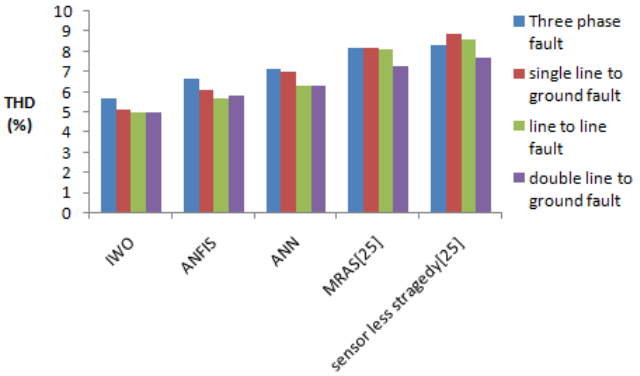

FIGURE 30. Graphical comparative THD (%) of grid current with IWO, ANFIS, ANN, and different techniques [25].

MRAS [25], and sensor less stragedy [25] which is shown in Table 8. Such comparison is also reflected in Fig. 30.

It can be referred from Table 8 and Fig. 30 that least distortion or THD (%) is found to be minimum with IWO in comparison to ANFIS, ANN, MRAS [25], and sensor less stragedy [25]. From the brief comparative analysis, it can be concluded that implication of IWO in sensor less control of DFIG gives best result with respect to other methods under balanced as well as unbalanced conditions.

VIII. CONCLUSION

This article presents the sensor less speed control of DFIG under the balanced and unbalanced conditions in a grid integrated system. Initially, the model of wind-driven DFIG has been developed. Thereafter different controllers like IWO, ANFIS, and ANN are designed and applied for the performance analysis of sensor less speed control of DFIG under both balanced and unbalanced conditions. It is observed that performance parameters like settling time and peak overshoot for sensor less speed of DFIG are found to be less with IWO in comparison to ANFIS, ANN, and other existing techniques. The unbalanced condition is represented by a three-phase fault, single line to ground fault, line to line fault, and double line to ground fault. It is also observed that tripping of fault

TABLE 9. Internal Parameters of DFIG.

15KW, 415V, 50Hz, 6 pole, H=0.385	
Parameters	**Value**
Resistance of stator(R_s)	0.023 pu
Inductance of stator (L_s)	0.18 pu
Resistance of rotor(R_r)	0.016 pu
Inductance of rotor(L_r)	0.16 pu
Mutual Inductance(L_m)	0.14 pu
DC link capacitance(C)	0.9 pu

currents and approaches to its healthy state with minimum distortion (THD) are found to be better with IWO in comparison to ANFIS, ANN, and other existing techniques. Such implication of the IWO technique makes the system highly robust and efficient.

APPENDIX

See Table 9.

REFERENCES

[1] J. Liu, "Impact of power grid strength and PLL parameters on stability of grid-connected DFIG wind farm," *IEEE Trans. Sustain. Energy*, vol. 11, no. 1, pp. 545–557, May 2020.

[2] F. Cheng, L. Qu, W. Qiao, C. Wei, and L. Hao, "Fault diagnosis of wind turbine gearboxes based on DFIG stator current envelope analysis," *IEEE Trans. Sustain. Energy*, vol. 10, no. 3, pp. 1044–1053, Jul. 2019.

[3] Z. Huang, Z. Wang, and L. Liu, "A practical fault diagnosis algorithm based on aperiodic corrected-second low-frequency processing for microgrid inverter," *IEEE Trans. Ind. Informat.*, vol. 15, no. 7, pp. 3889–3898, Jul. 2019.

[4] W. Xu, K. Yu, Y. Liu, and J. Gao, "Improved coordinated control of standalone brushless doubly fed induction generator supplying nonlinear loads," *IEEE Trans. Ind. Electron.*, vol. 66, no. 11, pp. 8382–8393, Nov. 2019.

[5] H. Huang, "Phase-amplitude model for doubly fed induction generators," *J. Mod. Power Syst. Clear Energy*, vol. 7, no. 2, pp. 369–379, Aug. 2019.

[6] S. K. Tiwari, B. Singh, and P. K. Goel, "Design and control of autonomous wind–solar system with DFIG feeding 3-phase 4-wire loads," *IEEE Trans. Ind. Appl.*, vol. 54, no. 2, pp. 1119–1127, Apr. 2018.

[7] Z. Fan, G. Song, X. Kang, J. Tang, and X. Wang, "Three-phase fault direction identification method for outgoing transmission line of DFIG-based wind farms," *J. Mod. Power Syst. Clear Energy*, vol. 6, no. 1, pp. 1–10, Jun. 2018.

[8] S. Yan, A. Zhang, H. Zhang, J. Wang, and B. Cai, "Transient stability enhancement of DC-connected DFIG and its converter system using fault protective device," *J. Mod. Power Syst. Clean Energy*, vol. 5, no. 6, pp. 887–896, Nov. 2017.

[9] S. G. Varzaneh, M. Abedi, G. B. Gharehpetian, and A. A. Suratgar, "Enhancement of output power smoothing and transient stability of DFIG-based wind energy conversion system using optimized controllers parameters," *Electr. Power Compon. Syst.*, vol. 45, no. 7, pp. 726–738, Apr. 2017.

[10] S. Demirbas, "Self-tuning fuzzy-PI-based current control algorithm for doubly fed induction generator," *IET Renew. Power Gener.*, vol. 11, no. 13, pp. 1714–1722, Nov. 2017.

[11] M. Doumi, I. Colak, A. G. Aissaoui, M. Abid, and A. Tahour, "Robust MRAC for a wind turbine based on a doubly-fed induction generator," in *Proc. IEEE 6th Int. Conf. Renew. Energy Res. Appl. (ICRERA)*, Nov. 2017, pp. 1160–1165.

[12] A. El Yaakoubi, K. Attari, A. Asselman, and A. Djebli, "Novel power capture optimization based sensorless maximum power point tracking strategy and internal model controller for wind turbines systems driven SCIG," *Frontiers Energy*, vol. 13, no. 4, pp. 742–756, Dec. 2019.

[13] N. Kumar, T. R. Chelliah, and S. P. Srivastava, "Impact of unbalance grid voltage on the performance of doubly-fed induction machine at motoring mode," *Electr. Power Compon. Syst.*, vol. 44, no. 11, pp. 1291–1306, Jul. 2016.

[14] L. Yang, Z. Xu, J. Ostergaard, Z. Y. Dong, and K. P. Wong, "Advanced control strategy of DFIG wind turbines for power system fault ride through," *IEEE Trans. Power Syst.*, vol. 27, no. 2, pp. 713–722, May 2012.

[15] Y. Bekakra and D. B. Attous, "DFIG sliding mode control fed by back-to-back PWM converter with DC-link voltage control for variable speed wind turbine," *Frontiers Energy*, vol. 8, no. 3, pp. 345–354, Sep. 2014.

[16] R. Cheikh, A. Menacer, and S. Drid, "Robust control based on the Lyapunov theory of a grid-connected doubly fed induction generator," *Frontiers Energy*, vol. 7, no. 2, pp. 191–196, Jun. 2013.

[17] A. Karthikeyan, C. Nagamani, A. B. R. Chaudhury, and G. S. Ilango, "Implicit position and speed estimation algorithm without the flux computation for the rotor side control of doubly fed induction motor drive," *IET Electr. Power Appl.*, vol. 6, no. 4, pp. 243–252, Apr. 2012.

[18] M. Singh and A. Chandra, "Application of adaptive network-based fuzzy inference system for sensorless control of PMSG-based wind turbine with nonlinear-load-compensation capabilities," *IEEE Trans. Power Electron.*, vol. 26, no. 1, pp. 165–175, Jan. 2011.

[19] H. M. Jabr, D. Lu, and N. C. Kar, "Design and implementation of neuro-fuzzy vector control for wind-driven doubly-fed induction generator," *IEEE Trans. Sustain. Energy*, vol. 2, no. 4, pp. 404–413, Oct. 2011.

[20] B. Singh, S. K. Aggarwal, and T. C. Kandpal, "Performance of wind energy conversion system using a doubly fed induction generator for maximum power point tracking," in *Proc. IEEE Ind. Appl. Soc. Annu. Meeting*, Oct. 2010, pp. 1–7.

[21] J. Yao, H. Li, Y. Liao, and Z. Chen, "An improved control strategy of limiting the DC-link voltage fluctuation for a doubly fed induction wind generator," *IEEE Trans. Power Electron.*, vol. 23, no. 3, pp. 1205–1213, May 2008.

[22] W. Qiao, W. Zhou, J. M. Aller, and R. G. Harley, "Wind speed estimation based sensorless output maximization control for a wind turbine driving a DFIG," *IEEE Trans. Power Electron.*, vol. 23, no. 3, pp. 1156–1169, May 2008.

[23] O. A. Mohammed, Z. Liu, and S. Liu, "A novel sensorless control strategy of doubly fed induction motor and its examination with the physical modeling of machines," *IEEE Trans. Magn.*, vol. 41, no. 5, pp. 1852–1855, May 2005.

[24] R. K. Behera and W. Gao, "A novel controller design for grid-side converter of doubly fed induction generator for wind power interface: An experimental investigation," *Electr. Power Compon. Syst.*, vol. 38, no. 14, pp. 1531–1545, Dec. 2010.

[25] A. Izanlo, S. A. Gholamian, and M. V. Kazemi, "Comparative study between two sensorless methods for direct power control of doubly fed induction generator," *Rev. Roum. Sci. Techn., Électrotechn. et Énerg*, vol. 62, no. 4, pp. 358–364, 2017.

ABHINAV SAXENA (Member, IEEE) was born in Farrukhabad, Uttar Pradesh, India. He received the B.Tech. degree in electrical engineering from UPTU, Lucknow, in 2011, the M.Tech. degree from IIT Roorkee, in 2013, and the Ph.D. degree in electrical engineering from Jamia Millia Islamia, New Delhi, India, in 2020. He is currently working as an Assistant Professor with the Department of Electrical Engineering, JSSATE Noida (AKTU), Uttar Pradesh. He has more than 50 research papers and ten published patent. He is also having a project of Rs. five Lakhs. He is co-supervising three Ph.D. students. His research interests include power electronics, electrical machines, power systems, control system and intelligent techniques, renewable energy, non-linear controller, smart grid, DG, DER, electric vehicle, congestion management, DG, energy management, controling through intelligent technique, and analysis of biological equipment.

RAJAT KUMAR (Member, IEEE) received the B.Tech. degree in electrical and electronics engineering from Uttar Pradesh Technical University, Lucknow, India, in 2013, the M.Tech. degree (Hons.) in power electronics and drives from the Madan Mohan Malaviya University of Technology, Gorakhpur, India, in 2017, and the Ph.D. degree from the Sant Longowal Institute of Engineering and Technology, Longowal, Punjab, India, in 2021. He is currently the DST Government of India AWSAR Award Winner, in 2019. He is also an Assistant Professor with the Electrical and Electronics Engineering Department, Vardhman College of Engineering, Shamshabad, Hyderabad, India. His current research interests include application of DSP and AI techniques in power systems and power electronics converter applications in renewable energy systems.

JAY SINGH (Senior Member, IEEE) received the B.Tech. degree in electrical engineering from IIT Dhanbad, the M.Tech. degree in electrical engineering from Maharshi Dayanand University, Rohtak, and the Ph.D. degree from MMMUT, Gorakhpur. He is currently working as an Associate Professor with the Department of Electrical and Electronics Engineering, G. L. Bajaj Institute of Technology and Management, Greater Noida, Uttar Pradesh, India. He is also the Coordinator of International & National Affairs, NBA, NAAC, and research and development activities. He has been awarded several times as best faculty. He has delivered 26 expert lectures in national and international programs. He has published 64 research papers in reputed international journals/conferences. He is a member of Strategy Planning Sub-Committee and IEEE UP Section India. Also, he is a member of four international technical societies and guest editor of two international journals.

GYANENDRA KUMAR SINGH received the Ph.D. degree in mechanical engineering from the M. N. National Institute of Technology, Allahabad, India, (an Institute of National Importance), in 2011. He is currently working as an Associate Professor with the Adama Science and Technology University, Adama, Ethiopia. He has over two decades of experience in Academics. He has published more than 70 research articles in international journals and conference. He holds a Lifetime Membership of the Indian Society of Technical Education. His research interests include the interdisciplinary field of materials science, but they are not limited to smart materials, such as 4D printed materials, self healing composites and bio functional nanofibers, and the modeling and optimization of modern manufacturing processes.

V. SAMPATH KUMAR received the B.E. degree in electronics and communication engineering, the M.Tech. degree in VLSI design, and the Ph.D. degree in semiconductor memory design. He is currently working as an Assistant Professor with the Department of Electronics and Communication Engineering, JSS Academy of Technical Education, Noida, India. He has published more than 50 papers in national and international journals and conferences, four patents, and handling currently two research projects. His research interests include VLSI design, reconfigurable memory design for low power SoC applications, semi or full-custom chips for implementation of specific architecture, and digital design.

J. P. PANDEY received the B.Tech. degree in electrical engineering and the M.Tech. degree in electrical engineering—power systems from KNIT, Sultanpur, Uttar Pradesh, India, and the Ph.D. degree from UPTU, Lucknow, under the supervision of Dr. D. S. Chauhan. He was worked as the Director of KNIT, Sultanpur. He is currently a Former and the Founder Vice Chancellor. He is also the Vice Chancellor of MMMUT, Gorakhpur, and a Professor with the Department Electrical Engineering Department, KNIT, Sultanpur. He has more than 30 years of experience in the field of teaching, industry, and administration. He has published more than 30 technical papers in peer-reviewed journals, including IEEE and in conference proceedings, guided five Ph.D. scholars and has three patents. He is also guiding five Ph.D. scholars.